Open access • Journal Article • DOI:10.1115/1.4042024

Flame and Spray Dynamics During the Light-Round Process in an Annular System Equipped With Multiple Swirl Spray Injectors — Source link

Kevin Prieur, Guillaume Vignat, Daniel Durox, Thierry Schuller ...+1 more authors

Institutions: Université Paris-Saclay, University of Toulouse

Published on: 30 Aug 2018 - Journal of Engineering for Gas Turbines and Power-transactions of The Asme (American Society of Mechanical Engineers Digital Collection)

Topics: Flame structure, Combustor and Injector

Kevin Prieur
Laboratoire EM2C,
CNRS,
CentraleSupélec,
Université Paris-Saclay,
3, rue Joliot Curie,
Gif-sur-Yvette cedex 91192, France;
Safran Tech,
E&P,
Châteaufort,
CS 80112,
Magny-Les-Hameaux 78772, France

Guillaume Vignat[1]
Laboratoire EM2C,
CNRS,
CentraleSupélec,
Université Paris-Saclay,
3, rue Joliot Curie,
Gif-sur-Yvette cedex 91192, France,
e-mail: guillaume.vignat@centralesupelec.fr

Daniel Durox
Laboratoire EM2C,
CNRS,
CentraleSupélec,
Université Paris-Saclay,
3, rue Joliot Curie,
Gif-sur-Yvette cedex 91192, France

Thierry Schuller
Institut de Mécanique des Fluides de Toulouse,
IMFT,
Université de Toulouse, CNRS,
Toulouse, France

Sébastien Candel
Laboratoire EM2C,
CNRS,
CentraleSupélec,
Université Paris-Saclay,
3, rue Joliot Curie,
Gif-sur-Yvette cedex 91192, France

Flame and Spray Dynamics During the Light-Round Process in an Annular System Equipped With Multiple Swirl Spray Injectors

A successful ignition in an annular multi-injector combustor follows a sequence of steps. The first injector is ignited; two arch-shaped flame branches nearly perpendicular to the combustor backplane form; they propagate, igniting each injection unit; they merge. In this paper, characterization of the propagation phase is performed in an annular combustor with spray flames fed with liquid n-hepane. The velocity and the direction of the arch-like flame branch are investigated. Near the backplane, the flame is moving in a purely azimuthal direction. Higher up in the chamber, it is also moving in the axial direction due to the volumetric expansion of the burnt gases. Time-resolved particle image velocimetry (PIV) measurements are used to investigate the evaporating fuel droplets dynamics. A new result is that, during the light-round, the incoming flame front pushes the fuel droplets in the azimuthal direction well before its leading point. This leads to a decrease in the local droplet concentration and local mixture composition over not yet lit injectors. For the first time, the behavior of an individual injector ignited by the passing flame front is examined. The swirling flame structure formed by each injection unit evolves in time. From the ignition of an individual injector to the stabilization of its flame in its final shape, approximately 50 ms elapse. After the passage of the traveling flame, the newly ignited flame flashbacks into the injector during a few milliseconds, for example, 5 ms for the conditions that are tested. This could be detrimental to the service life of the unit. Then, the flame exits from the injection unit, and its external branch detaches under the action of cooled burnt gases in the outer recirculation zone (ORZ). [DOI: 10.1115/1.4042024]

1 Introduction

Ignition of gas turbines and aeronautical engines is a major engineering issue. To tackle the high ignition reliability requirements, their combustors, most often annular in shape, are equipped with two or more spark plugs that are placed near the backplane. The first step of the ignition process is the initiation of a hot gas core by the spark plugs. Second, the kernel volume increases in size and is convected to an injector unit igniting a first flame. As this flame is established, two traveling flames are initiated in the clockwise and counter-clockwise directions. These two flame branches propagate in the annular chamber, successively igniting different injectors. At a later stage, the two traveling flames merge. This entire process is called the light-round.

A detailed review of the literature is not the point of this paper as it is already available in Ref. [1]. However, it is worth noting that experiments in multi-injector systems have been carried out more recently with linear arrangements [2,3] or annular configurations that come closer to the industrial geometries [4–6]. Important progress has been made in the past years with a pioneering demonstration of the Large Eddy Simulation of a helicopter combustor [7] and some recent calculations of full annular geometries pursue this effort [8–12]. Experimental results have been well retrieved in some of these calculations [8–10] in the premixed gaseous fuel case. Experiments with liquid fuel injection in annular systems are less well documented with the exception of Ref. [1] where *n*-heptane is injected in the airflow. These experiments were performed in a laboratory scale apparatus called multiple injector combustor for combustion dynamics and acoustic analysis (MICCA)-spray with sixteen swirl spray injectors and an annular geometry in a configuration close to the situation prevailing in real systems. The ignition process has been studied under premixed gaseous propane air conditions and with

[1]Corresponding author.

liquid *n*-heptane and *n*-dodecane injections. Light-round time delays have been extensively characterized for these configurations. It has been shown that the propagation speed of the flame in the annulus mainly depends on three factors: the thermal expansion, the turbulent flame wrinkling, and the laminar burning velocity in the spray reactive mixture.

This paper pursues the analysis of the light-round process and deals with the circular propagation of the flame in the annular space defined by the chamber sidewalls. Most of the studies reviewed previously have mainly concerned the time delay between the initiation of the flame kernel close to the spark plug and the merging of the two flame branches that travel in the annulus. However, one important issue is to see how each flame is initiated at one of the injector units. This takes place when one of the traveling flames sweeps one of these units. The dynamical process that produces the flame and leads to its final anchoring is of considerable importance but does not seem to be well documented in the previous literature. The objective of this paper is twofold. Flame arch propagation and liquid fuel droplet velocities in front of the traveling flame are first examined during the light-round process. Data are then reported from experiments on a process where one injector is ignited by the traveling flame front.

The paper is organized as follows. After a brief description of the experimental setup in Sec. 2, data gathered in light-round experiments are discussed in Sec. 3. This section focuses on the velocity fields in the vicinity of the flame as it moves around the circumference. Section 4 is concerned with observations of the flame structure as it evolves after the flame has swept an injector. It is shown that the flame initially penetrates in the injector body and is later expelled from this position to find its final configuration after a relatively long period of time. A mechanism of this type is also observed in the case of ignition of a single swirling injector of the same type as those used in the MICCA-spray experiment. The results on this single injector are analyzed in Sec. 5. Several mechanisms that may be involved in this transient flame behavior are presented in Sec. 6. An attempt is finally made to model the injector dynamical response when it is swept by the flame and describe the resulting consequences in terms of mass flowrate and subsequent flame motion.

2 Experimental Configuration

The experimental setup shown in Fig. 1 comprises an annular plenum and an annular combustion chamber. The plenum and the chamber are linked by an annular plate equipped with sixteen injectors. Eight channels feed the plenum with pure air injected at ambient temperature. The flow is set in a rotating motion in each injector by a tangential swirler comprising six 3 mm diameter holes resulting in a swirl number $S \approx 0.65$. More details are given in Ref. [1].

Liquid *n*-heptane is injected in the chamber by a simplex atomizer with an orifice placed on the downstream side of the swirler, 6 mm in recess with respect to the injector outlet. This atomizer establishes a hollow cone spray in the chamber. Ignition is initiated by a spark plug positioned approximately at 10 mm from the center of one injector as depicted in Fig. 1. The lateral chamber walls are formed by two cylindrical quartz tubes of 200 mm length. The inner and outer walls have, respectively, a diameter of 300 mm and 400 mm.

The system is equipped with twelve 1/4 in. Brüel and Kjäer microphones to measure the acoustic pressure in the plenum and in the chamber at a sampling rate $f_s = 32{,}768$ Hz. This value is much larger than the maximum frequency of these signals and no filtering is applied to the data except when this is mentioned. Eight of the microphones designated as "MC" (chamber microphone) are used to measure the pressure at the chamber backplane. The pressure taps drilled in the annular chamber base (Fig. 1, middle) are located at equal distance from two injectors and connected to straight metallic waveguides crossing the plenum and terminated by a 25 m long flexible tube closed at its extremity. Each MC microphone is flush mounted on a waveguide at 170 mm from the chamber backplane. This distance defines a time lag $\tau_{m-b} = 0.46$ ms when the combustion chamber has been running for 15 min, and the temperature in the plenum reaches 55 °C. This delay between the chamber and the microphone is taken into account to synchronize the acoustic pressure measurements. Four additional microphones designated as "MP" (plenum microphone) are plugged on the plenum, flush to its wall.

Images of the combustion region are recorded by a high-speed camera Phantom V2512 providing 16-bit images covering 1280×800 pixels at a sampling rate of 6000 frames per second, with a shutter duration of 166 μs. Images are filtered to subtract the large infra-red and red components of the emission of the quartz tubes heated up at 900 K. Depending on the experiment, the camera is equipped with an optical filter, either a broadband filter centered on CH* emission (400–470 nm) with a high transmission factor (0.8) to capture the flame luminosity in this band, or, when a laser is used, a broader filter (300–680 nm). For some experiments, a thin metallic plate is placed in the center of the annular chamber perpendicular to the camera to block the luminosity from one of the flame arches when looking at the other (see Fig. 1, middle). The pressure signals and flame images can be synchronized by making use of the external triggering signal of the camera.

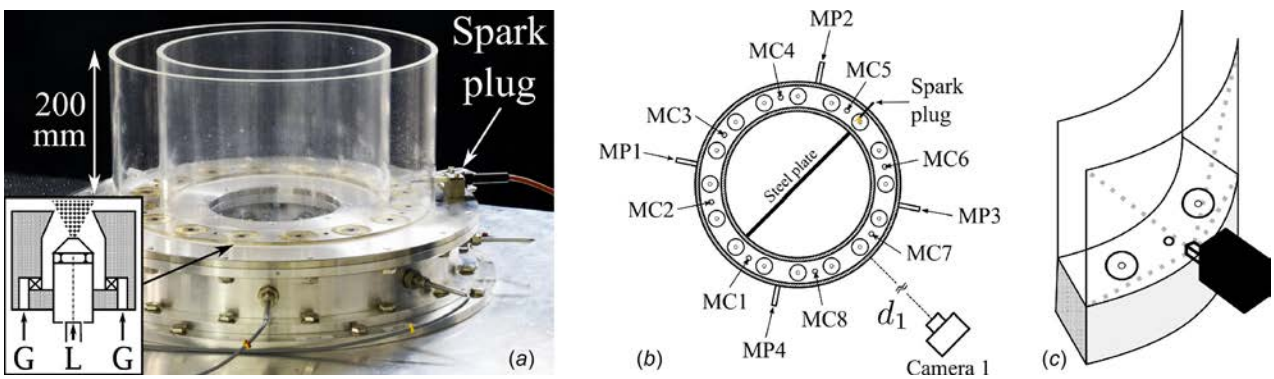

Fig. 1 Left: photograph of the MICCA-spray annular combustor with sixteen liquid spray injectors. A detailed schematics of the injector is available on the bottom left of the image. Middle: schematic view of the chamber backplane showing the locations of the camera and of different microphones MCx (chamber microphone n°x) in the chamber and MPx (plenum microphone n°x) in the air plenum. The spark plug location is indicated and defines flame 1. A steel plate is added in the center to block the luminosity of the opposite flame branch. The aim of the camera is either one injector or between two injectors, depending on the experiment. Right: view of the position of the camera in black with a cut of two sectors of the annular combustor. The gray-dashed lines symbolize the field of view of the camera.

The MICCA-spray chamber features 16 stable flames for *n*-heptane fuel injection over a wide range of operating conditions. The sixteen turbulent flames have a typical "M" shape without any visible mutual interaction once established. The system can be operated over a wide range of operating conditions with different fuel types. Experiments reported in this paper are carried out for one specific nominal condition where the global equivalence ratio is $\phi = 0.89$, the total power is $\mathcal{P} = 80\,\text{kW}$, and the bulk velocity at the exit of the injector is $U_b = 31\,\text{m s}^{-1}$. The Reynolds number based on the injector exit diameter is in this case 15,900 underlying the high turbulence levels obtained. For most of the data presented in this paper, the chamber is preheated for 10 min before initiating the light-round. The chamber external wall reaches 870 K where the temperature is measured, i.e., between two flames, on the outer part of the quartz cylinder, 100 mm from the chamber backplane. As reported in Ref. [1], the thermal conditions have a notable influence on the light-round process.

As suggested by a reviewer, the flow and light-round patterns in the real engine case with a turbine at the end of the combustor may differ from the ones observed in this paper where the combustor has an open-end. In particular, the burner dynamics during light-round could be different if an exit blockage is present as the sudden volume expansion would then lead to a reverse flow inside the burner. But, we can point out that, during the ignition sequence, the flow is not established in the combustor. As a consequence, the outlet is probably closer to an open end than to a choked nozzle. These observations justify the choice made in the present experiment.

3 Light-Round Experimental Data and Interpretation

An analysis of the images of the traveling flame branch (TFB) viewed from the side of the MICCA-spray system is first carried out. The evolution in flame structure and shape of individual flames formed after the passage of the TFB is then discussed in Sec. 4.

3.1 Flame Front Passage Ninety Degrees From the Ignition Point During the Light-Round. The high-speed camera is placed on the side of the annular combustor facing the region between two injectors (see Fig. 1). The optical axis is at the level of the backplane of the chamber. This is used to observe one branch of the flame during the light-round as shown in Fig. 2. The time instants are counted with respect to an initial time $t = 0\,\text{ms}$ when the spark plug initiates a flame kernel at the first injector. The flame then propagates from right to left in the sequences of images displayed in this figure. These images provide information on the flame propagation during the process as it will be investigated in the next paragraphs. The structures that are observed in Fig. 2 can be used to estimate the propagation speed of the flame front using particle image velocimetry (PIV) algorithms. The camera runs at 6000 Hz which is, of course, not enough to sample the displacement of PIV particles, but the motion of the large structures characterizing the flame is well captured at this frame rate. Open source PIV software such as PIVlab [13], interfaced with MATLAB, can then be used to determine the velocity of these structures. Images are first post-processed using adaptive histogram equalization (20 pixels) and high-pass filtering (15 pixels) to enhance the flame structures. FFT window deformation algorithms are then applied with two passes with a final interrogation window of 32×32 pixels interpolated with spline functions. A 2×3-point Gaussian shape fitting is then used for the sub-pixel estimation. The velocity field (u_θ, u_z) is superimposed to the flame front propagation in Fig. 3 with u_z being the axial velocity and u_θ the azimuthal component. This last component is in fact an estimation of the azimuthal velocity as the flame propagation is curved due to the annular shape of the chamber. This deviation is small as the radius of curvature is large. Velocity vectors are spatially filtered in order to be calculated where well-defined flame structures are found.

One observes, in Fig. 3, that the velocity fields may be divided into regions I and II where the velocity orientations are distinct. In region I, the velocity of the flame front is purely azimuthal with essentially no axial component. There, the traveling flame is stuck to the chamber backplane and moves forward in the azimuthal direction from one injector to the next. This indicates that zone I is the part of the flame front responsible for the ignition of the eight injectors on its path covering half of the annular chamber. Velocities in this region can be estimated from different instantaneous images. One obtains a mean velocity v_θ comprised between 15 and 20 m s^{-1} for zone I.

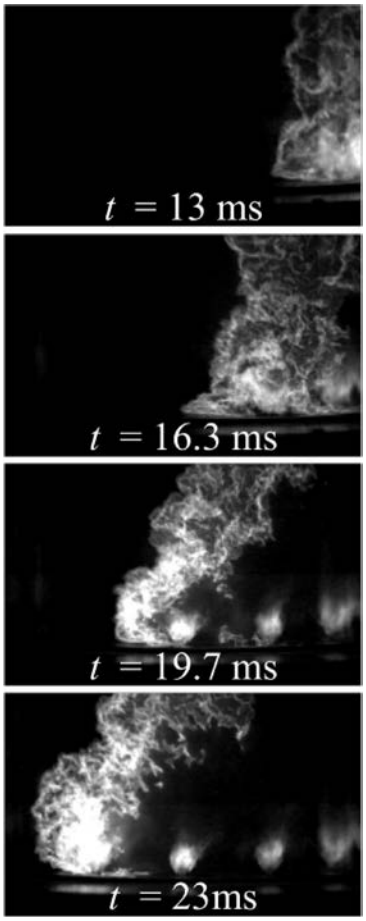

Fig. 2 Passage of the traveling flame at four different instants during the light-round. The camera is placed on the side of the combustor and its optical axis is at the level of the chamber backplane. The luminosity of the other flame branch propagating in the other half of the annular combustor is blocked by a steel plate placed in the central plane of the system. The origin of time $t = 0$ ms corresponds to the ignition of a hot kernel by the spark plug. In the bottom image, one can see three different ignited injectors, while one other injector is being swept by the traveling flame front.

Zone II corresponds to the region where the flame is propagating azimuthally and axially due to the burnt gases expanding and pushing the reactive front toward the exit of the combustion chamber. In this region, the velocity magnitude is estimated to be in the range 10–15 m s^{-1}, confirming the trend that the leading point of the flame propagation is close to the chamber backplane. This type of propagation consists in a burner-to-burner propagation and has already been discussed in some previous articles [4,5]. This feature is also observed numerically in full annular light-round large eddy simulations [11].

3.2 Behavior of the Droplet Cloud During the Light-Round Process. In a follow-up experiment, a 1.5 W continuous 532 nm laser is used to generate a vertical slice approximately 2 mm wide. The laser light beam crosses the outer quartz tube and

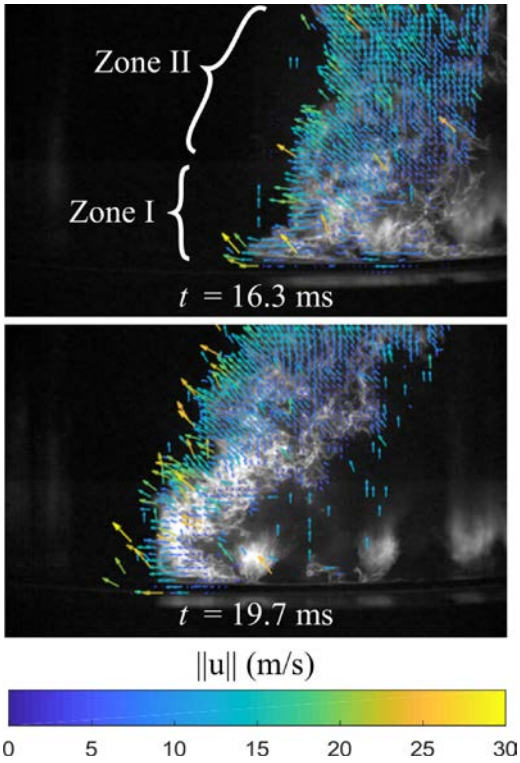

Fig. 3 Result of a PIV processing of the flame passage at two different instants during the light-round. Regions I and II correspond to different flame propagation behaviors and are explained in the text. The origin of time $t = 0$ ms corresponds to the ignition of a hot kernel by the spark plug. Velocity vectors are colored by their magnitude using the colormap inserted below the images. See online figure for color.

forms a vertical sheet that is perpendicular to the line of sight of the camera. The slice contains the axis of one injector. Figure 4 shows two nonconsecutive images recorded at 6000 Hz. One can see that the laser slice features striations due to the crossing of the 6 mm-thick quartz tube. This cannot be easily corrected since the tube thickness is necessary to sustain the high-temperature combustion conditions. In this experiment, the chamber walls had to be maintained cold in order to obtain a sufficient number of droplets to be visualized. If the walls were preheated as in all other experiments, the evaporation of the liquid *n*-heptane would have been too fast and no droplet would have remained a few centimeters downstream the injector exit.

Top images in Fig. 4 show the behavior of the *n*-heptane droplets when the flame is sufficiently far from the injector and when it approaches this unit. At $t = 5$ ms, the droplets appear as brilliant point sources, indicating that they are nearly still. At $t = 11.7$ ms, the flame front approaches from the right side of the image. Note that the flame front is not clearly identified due to the high luminosity of the droplets. In contrast with the previous image, droplets are globally displaced to the left, spray zones are densified whereas other zones feature a lower fuel load when the two images are compared. PIV algorithms are again applied to the *n*-heptane droplets to deduce the velocity field of the liquid fuel.

Images showing the corresponding velocity vector fields are at the bottom of Fig. 4. In the left image, all the vectors have either a global axial component or show droplets trapped in the recirculation regions. This trend is then strongly perturbed when the flame front arrives from the right. Two regions can be clearly identified. Zone A is where the droplets are not affected by the incoming flame front. Zone B is the region where the liquid fuel is influenced by the incoming flame front. Part of the droplets is displaced to the left with an estimated velocity of 5–10 m s^{-1}. Note that these values are lower than those found for the velocity of the flame front in Fig. 3. This is so for two reasons. First, the droplets have their own inertia and the flame front is advancing faster and consuming the *n*-heptane droplets. Second, flame velocities are lower because of the cold walls that increase the light-round time delay. This droplet motion is the result of the piston effect induced by the flame on the fresh gases flowing on its upstream side as discussed in Ref. [5]. These measurements yield clues on the distance of influence of the traveling flame branch. Taking into account all the available images, this distance is approximately equal to the spacing between two injectors $s = 68$ mm. This value of course depends on the configuration and ignition conditions. Note that this phenomenon can have a strong impact on the ignition sequence as it will change the concentration of liquid droplets, thus modifying the local equivalence ratio. Rich regions may

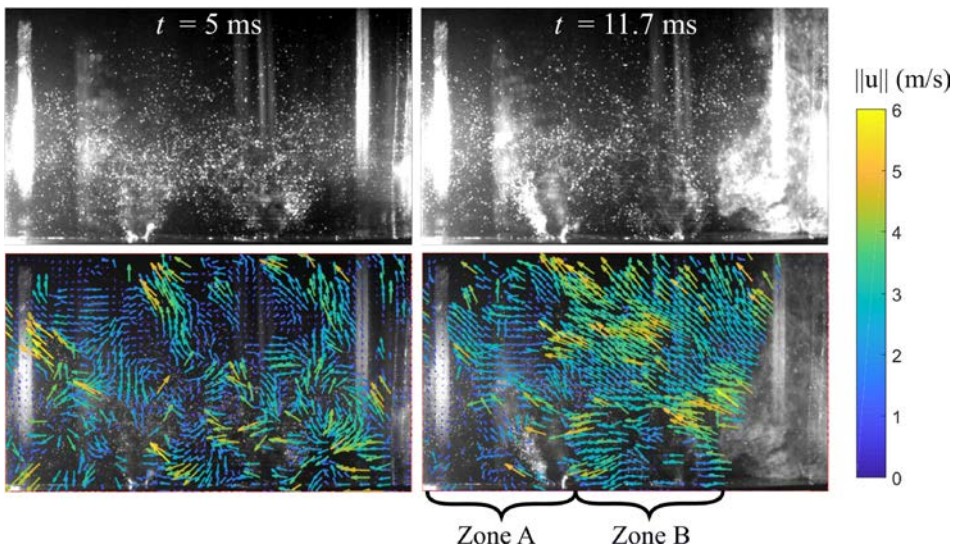

Fig. 4 Top: Images of the flame propagation with a laser slice to visualize the motion of the droplet spray. Camera position is given in Fig. 1. Bottom: Velocity fields calculated using PIV on the *n*-heptane droplets. False vectors have been eliminated. The time origin $t = 0$ ms corresponds to the ignition of a hot kernel by the spark plug. Velocity vectors are colored by their magnitude using the colormap inserted on the right of the images. See online figure for color.

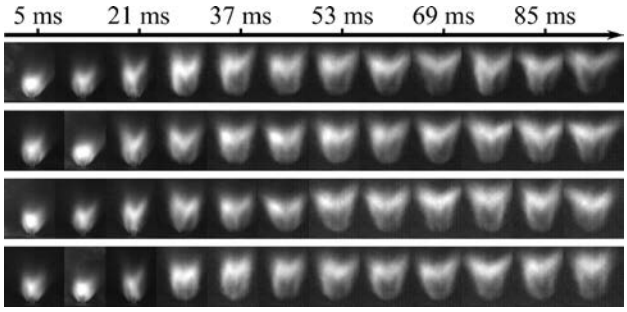

Fig. 5 Four ignition sequences showing the evolution of the time-averaged flame shape after the passage of the flame front. The time origin $t = 0$ ms corresponds to the instant when the injector is ignited by the incoming flame front.

appear inducing hot spots, while lean regions may form in other parts of the system eventually leading to a local reduction in combustion intensity.

One may ask whether the results depend on the relative position of the observation point. It turns out that the same features are recorded at nearly all injector positions. The flow configuration is, however, different near the spark plug where the flame is not fully established and near the location where the two traveling flame branches merge. In the final step before the merging, the flow is similar to that formed by two colliding streams near the stagnation point.

These effects of the flame on the droplet distribution have to be taken into account in models of the light-round in combustors using liquid fuels.

4 Flame Structure Evolution During the Light-Round

The high definition of the recorded images gives access to details of the flame shape during the ignition process of the annular chamber.

In order to reduce the noise due to turbulence induced fluctuations, 50 consecutive instantaneous images, corresponding to a short time period of 8.33 ms, are recorded and averaged to get moving-averaged filtered flame shapes. The filter size was chosen because the flame shape barely changes during this time scale. Figure 5 presents the filtered flame shape evolution of one injector for four different successful ignitions of the annular combustor. The initial time $t = 0$ ms corresponds to the ignition of this injector by the passing flame branch. One can see that the flame seems to be at first quite compact and close to the chamber backplane. The flame luminosity extends within the injection unit through the central recirculation zone. After 25 ms, it lifts off from the injector, expands in a clear M shape, and reaches its final position after 50 ms. This defines two time delays: τ_l between the time of ignition and the first flame shape switch, associated with the flame lift-off, and τ_f between the time of ignition and the stabilization of the flame in its final shape. On average, $\tau_l = 25$ ms and $\tau_f = 50$ ms.

The top of Fig. 6 shows two images of the flame 5 ms and 88 ms after the injector ignition. Luminosity levels are saturated in order to enhance the differences. One can see that the left flame is clearly attached to the lips of the injection unit and is even entering inside the injector, drawn in by the central recirculation zone formed by the swirling flow. After several milliseconds, the inner flame stabilized in the recirculation zone vanishes and the flame lifts off its anchoring points. Filtered Abel transform images are in both cases proposed in the lower part of Fig. 6, featuring two flame shapes "A" and "B." This phenomenon of upstream propagation of the flame front in the injector can be detrimental to the life duration of this unit. As the flame travels in the injector, internal metallic parts are exposed

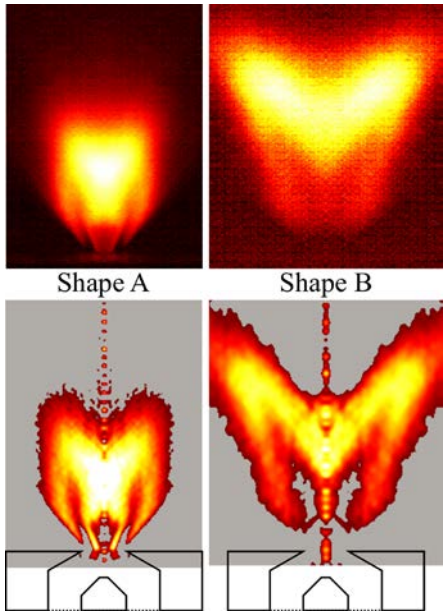

Fig. 6 Left: flame shape 5 ms after the flame front ignites this injector (top, shape A) and Abel transform of the flame (bottom, shape A). Right: flame shape 88 ms after the flame front ignites this injector (top, shape B) and Abel transform of the flame (bottom, shape B). Images are represented in false colors and saturated to highlight their different structures. Yellow and white correspond to high light intensities, while dark red represents low light emission levels. The Abel transform gives rise to errors in the near vicinity of the axis so that the values in this region should not be considered. See online figure for color.

to high temperatures. Although this takes place over a period of a few milliseconds, this thermal loading might degrade the injection components. It is worth noting that this process is repeatable and not specific to the configuration described in this paper. The Appendix reports the same phenomenon in a different configuration of the MICCA chamber [5] corresponding to a premixed propane and air injection system using a very different injector geometry.

It has been seen in the previous paragraphs that it takes approximately $\tau_l = 25$ ms to expel the flame from the injection unit and that an additional delay $\tau_f = 50$ ms is required for the flame to reach its final shape after ignition. Figure 7 shows time-averaged images of three different neighboring flames in the MICCA-spray chamber during the light-round. The averaging method over 8 ms is identical to the one used for images shown in Figs. 5 and 6. Flames are designated by letters "α," "β," and "γ," from right to left. The time-step between each mean image is approximately 17 ms. The initial instant $t = 0$ ms corresponds to the ignition of flame γ. Flame α is ignited first at $t = -8$ ms. In the first snapshot, one can see that flames α and β are adopting an A shape as described before. Flame γ is not perfectly ignited yet. At $t = 17$ ms, flame α switches to a B shape (see Fig. 6), while β and γ still feature an A shape. 17 ms later, flame β has switched to the B shape, while flame γ is in the process of lifting-off. At $t = 51$ ms, all the flames are lifted and have adopted the B shape.

In conclusion, one can see that all the flames do not switch simultaneously from A to B shapes. The time delay τ_p between these changes is the delay for the flame front to travel from one injector to the next. The distance between two injectors is $s = (1/16)\ \pi D = 68$ mm with D being the mean diameter of the chamber. If one considers that the flame front absolute velocity v_f is a constant with $v_f \approx 17$ m s^{-1} (see Fig. 3), the time delay τ_p is

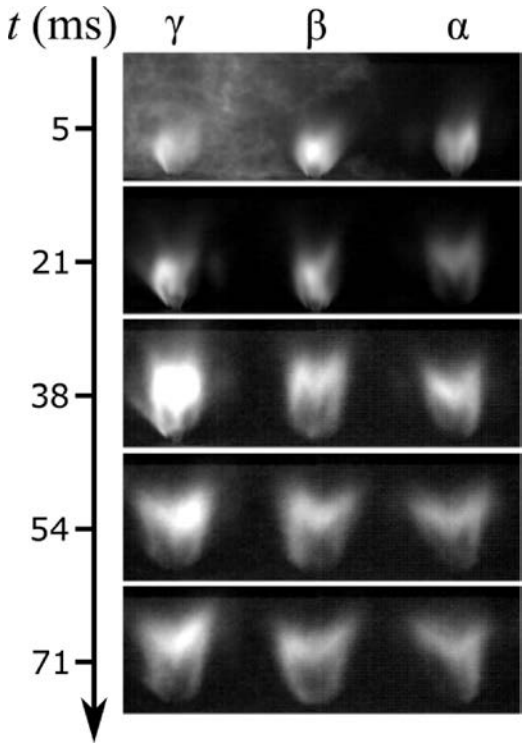

Fig. 7 Mean images of three consecutive flames of the annular combustor progressively switching from shape A to shape B. In the first image, the flame front propagates from right to left. The first flame to be ignited is flame α.

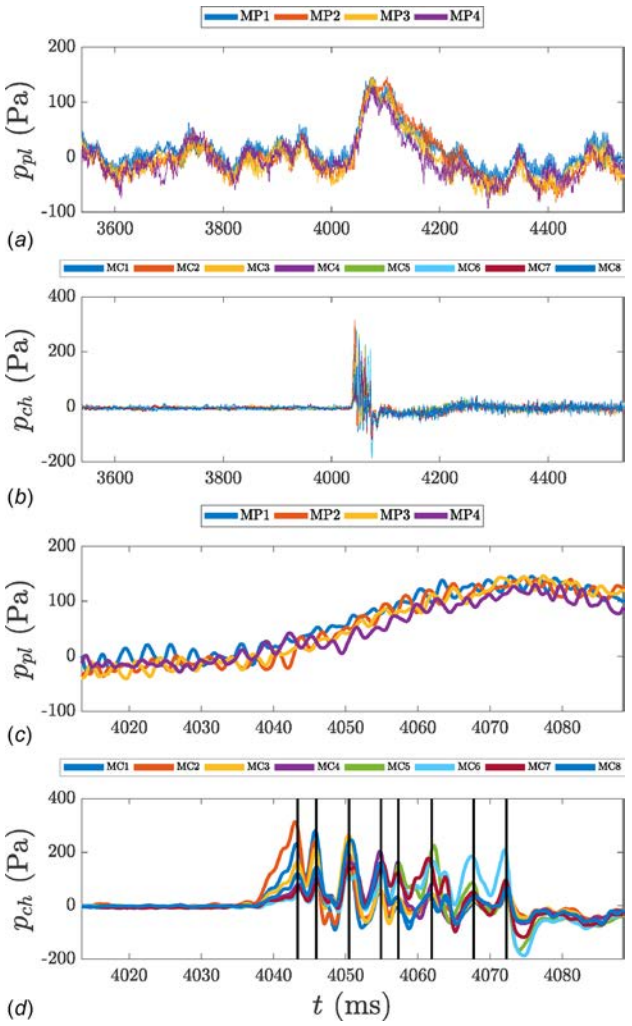

Fig. 8 Acoustic pressure recorded by four pressure sensors in the plenum (first and third graphs) and by eight pressure sensors in the chamber (second and fourth graphs) before and after the light-round. Note that the third and fourth figures are expanded views of the pressure tracks in the plenum and in the chamber during ignition. In the bottom graph, the black lines correspond to successive pressure peaks, each associated with the ignition of an injector. For clarity, the signals are low-passed filtered with a cutoff frequency of 500 Hz.

4 ms. In the annular combustor, the first flame ignited will lift-off and switch from A to B shape after $\tau = \tau_l = 25$ ms, whereas the second one will change after $\tau = \tau_l + \tau_p = 29$ ms. The n-th flame will then change after $\tau = \tau_l + (n-1)\tau_p$.

Acoustic pressure signals during the light-round process are recorded using four microphones "MPx" in the plenum and eight microphones "MCx" on the combustor backplane (see Fig. 1). Typical pressure signals are presented in Fig. 8. For this specific experimental run, ignition occurred shortly at $t = 4038$ ms. All plenum microphones show an initial rise in pressure to 130 Pa. This rise occurs over a duration of 40 ms, which corresponds to the light-round delay of the MICCA-spray combustor at this operating point. The key information to retrieve from Fig. 8 is that the pressure signals recorded by the chamber microphones MCx, each separated by 45 deg, appear to be in phase. One can see that the pressure wave arrives at nearly the same instant at every sensor positions in the bottom plot in Fig. 8 indicating that it propagates at the speed of sound c of the medium which is typically 720 m s^{-1} and which corresponds to a delay of 0.1 ms between two consecutive sensors. The pressure peaks in the bottom plot correspond to the ignition of the eight successive pairs of injectors in the annular combustor. This feature is underlined by different black vertical lines in the bottom figure. The peaks are all quasi-equally spaced in time and the delay is $\Delta t = 4$ ms which corresponds to the time for the traveling flame branch to propagate from one injector to the next.

5 Dynamics of Ignition in a Single Injector System

In order to investigate this transient flame structure and compare the behavior of one isolated injector and one flame in the annular MICCA-spray combustor during the ignition process, a single injector system, designated as single injector combustor for combustion dynamics and acoustic analysis (SICCA)-spray, is used. It is schematically shown in Fig. 9. It represents 1/16th of the MICCA-spray annular chamber. The surface of the quartz tube forming the combustion chamber is calculated to be close to the confinement of the flame in the annular device, and the same injection system is used. The resulting flame is similar in shape to that found in the annular chamber (not shown here). More details on the characterization of the flame in SICCA-spray are given in Ref. [1]. Air velocity measurements in the plenum are recorded with a hot wire located 100 mm upstream from the injector exhaust section. The plenum is carefully designed to generate a flat velocity profile at the hot wire position. The average velocity measured by the hot wire during steady operation at the nominal point is $u_0 = 2.06$ m s^{-1}. At this position, the section is round with a diameter of 30 mm. A photomultiplier (PM) tube with an optical filter centered on the wavelength of the emission of the OH* radical is used to estimate the unsteady heat release rate during ignition. It is worth noting that, even under these nonpremixed conditions, one may assume that the PM signal intensity provides to some extent an indication on the combustion intensity, which is linked to the flame luminosity. This was shown experimentally using a quasi-steady approach by Mirat et al. [14] and successfully applied in Ref. [15].

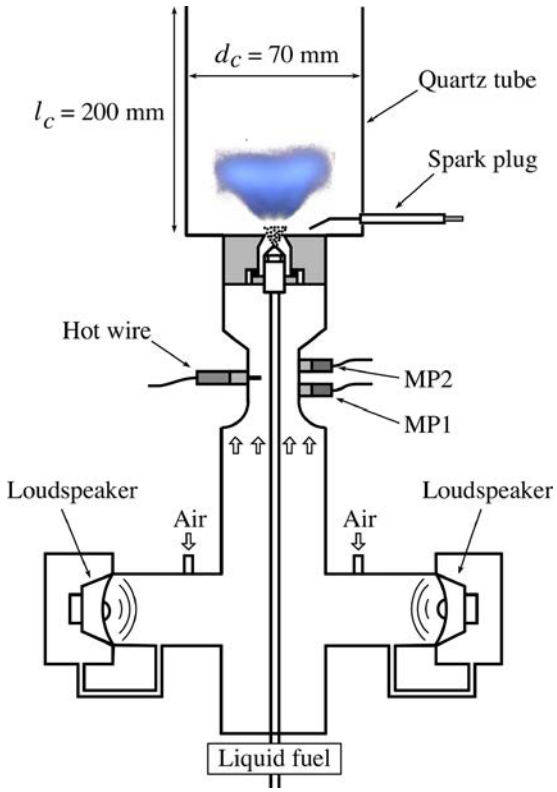

Fig. 9 Schematic representation of the SICCA-spray burner with key dimensions

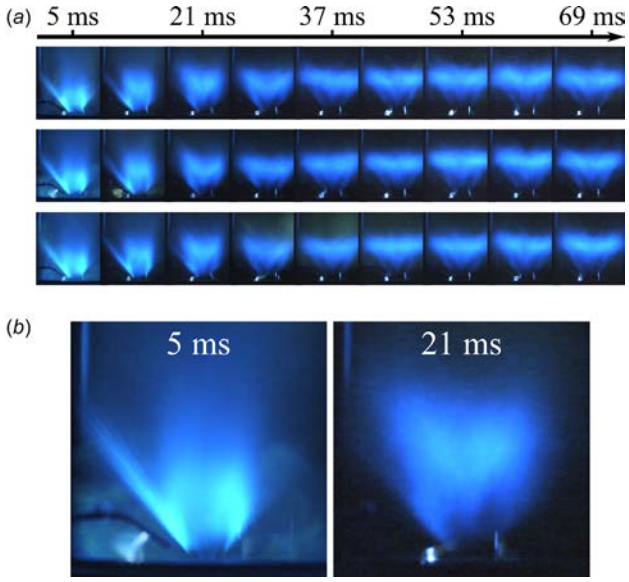

Fig. 10 Top: True-color ignition sequences in SICCA-spray. Bottom: Close-up images at $t = 5$ and 21 ms. Extra white luminosity is due to the sparks used to ignite the system, which are continuously operated at 100 Hz. See online figure for color.

In Sec. 4, it was found that the flame switched from shape A to shape B during the ignition of the annular chamber MICCA-spray. This feature was characterized by a lift-off time delay $\tau_l = 25$ ms. The stabilization of the flame in its final shape requires some more time, leading to an overall time delay of $\tau_f = 50$ ms for the flame to reach its final steady-state structure. The first step is to verify that the same features are found in the single injector system. Figure 10 presents three successful ignition runs. The same time-averaging method is used as for the data acquired in the annular chamber. One can see that the flame is first attached to the burner lips and quite compact, which can be identified as an A shape (Fig. 6). After roughly the same delay as in MICCA-spray, the flame detaches and adopts a B shape. This is confirmed by larger chemiluminescence images displayed in the bottom of Fig. 10.

Next, it is interesting to examine air velocity and flame luminosity measurements recorded simultaneously during several ignitions of the burner. Figure 11 presents typical results obtained during a period of 60 ms around the ignition time $t = 0$ ms. The high luminosity during the ignition process is due to the burning of all the fresh mixture in the chamber resulting in a saturation of the photomultiplier signal. The important information from this measurement is the instant at which the ignition begins. One can see in the plot that, as soon as the flame luminosity I begins to rise at $t = 0$ ms, the velocity at the hot wire decreases with a constant slope. This is best seen in the bottom plot where the velocity signal has been low pass filtered to eliminate a high-frequency periodic oscillation at 600 Hz already present before ignition and associated with an acoustic resonance in the combustor. The minimum value of velocity roughly drops down to around 1.55 m s^{-1}. The time of decay does not vary between each ignition and is equal to 4 ms on average (red dashed line in Fig. 11). After that, the air velocity then rapidly increases and overshoots above its mean value before stabilizing once again around it. This takes approximately 20–40 ms, defining the time delay τ_m, depending on the sequence. These time delays are of the same order of magnitude as τ_l the time delay required for flame lift-off in the MICCA-spray setup.

6 Mechanisms for the Flame Structure Evolution

In this section, physical mechanisms are examined to explain the flame shape evolution observed during the ignition in the two experimental setups MICCA-spray and SICCA-spray. It is first observed that just after ignition, the flame is initially located inside the injection unit within the central recirculation zone. At this time, a positive spike in the chamber pressure can be observed (see Fig. 8), as well as a drop in air flowrate (see Fig. 11). After a time delay $\tau_l = 25$ ms, the flame lifts-off and adopts the B shape described in Fig. 6. An additional time delay is necessary for the flame to take its final steady-state shape. This occurs with a delay $\tau_f = 50$ ms after ignition in the studied conditions.

Many phenomena can intervene to drive this process and control the transition in flame shape and location:

(1) The turbulent state of motion in the combustion zone, the equivalence ratio, and in the case of spray injection, the size of the fuel droplets.
(2) The aerodynamics of the injector flow.
(3) The thermal conditions in the flame region neighborhood.

The first two items control the flame penetration inside the injector unit, while the third most probably determines the transition from this initial configuration to the final state where the flame is stabilized at a distance from the injector exhaust. This is examined in more detail in what follows.

6.1 Equivalence Ratio and Turbulence Effects. Concerning the first set of factors, the fuel mass flowrate is most probably not affected by the ignition as the pressure loss in the fuel line is around 10 bar. However, it was shown in Sec. 3.2 that the traveling flame branch, while sweeping a new injector, perturbs the cloud of liquid fuel droplets, leading to an increase in the concentration of droplets and a locally richer mixture. The decrease in air

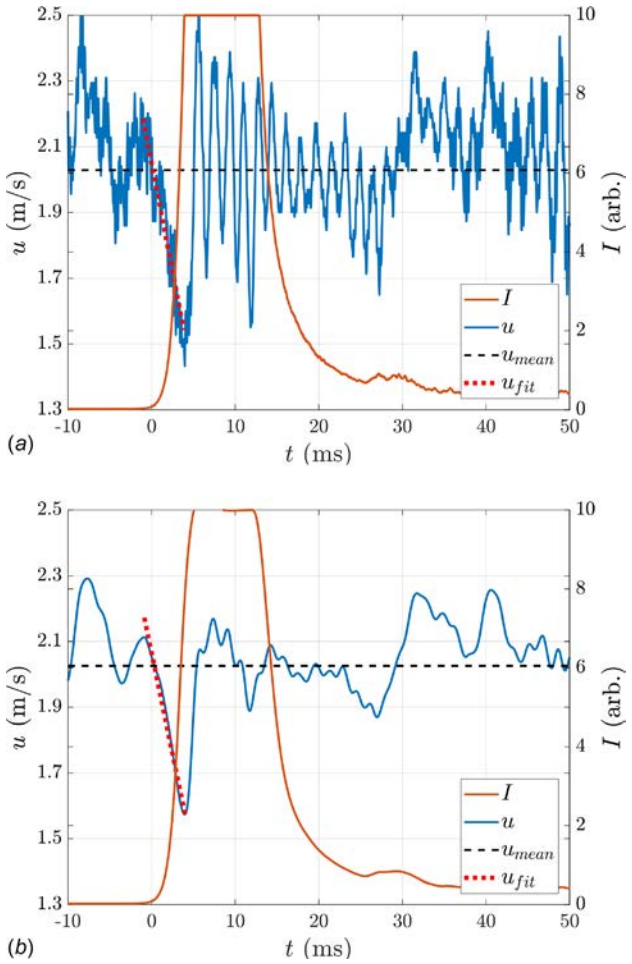

Fig. 11 Top: Velocity *u* and flame luminosity *I* signals during ignition of the single SICCA-spray injector. The black-dotted line corresponds to the mean velocity at nominal operating conditions. The red dotted line is a linear regression of the measured air velocity. Bottom: The signals are processed using a Butterworth low pass filter at 200 Hz, underlining the sudden decrease of the flowrate and its readjustment after the flame passage. See online figure for color.

mass flowrate through the injection unit is also conducive to locally richer fuel–air mixtures in the instants following ignition. As the combustor is operated at an overall lean condition, this increase in fuel–air ratio will lead to an increase in laminar burning velocity.

Two delays related to the behavior of the droplets are particularly relevant in this context: the convection time of a droplet through the flame τ_{cf} and the droplet lifetime before complete evaporation τ_{vap}. The first delay τ_{cf} is the ratio between the length of the flame and the bulk velocity: $\tau_{cf} = l_f/u_b = 2$ ms. The droplet lifetime was evaluated in Ref. [16] at $\tau_{vap} = 0.8$ ms for droplets having a Sauter mean diameter typically found in MICCA-spray. These delays are relatively small compared to the 50 ms required for the change in flame shape. Furthermore, the results from the premixed propane-air configuration presented in Appendix indicate that the effects of the spray are probably not driving the change in flame shape.

Turbulence in the combustion zone at the outlet of the injector will also affect the turbulent burning velocity. Following ignition and the subsequent rise in gas temperature, the turbulence level is likely to decrease, leading to lower turbulent burning velocity and local combustion intensity. The flame will have a reduced capacity to lie in the high velocity region inside the injector unit but this effect remains difficult to quantify.

6.2 Flow and Injector Dynamics. The injector flow dynamics is perturbed by the rise in pressure observed in Fig. 8 that occurs in the injector vicinity just after ignition. This pressure perturbation is associated with the rate of change of the heat release rate and can be estimated using the following equation:

$$p'(\boldsymbol{r},t) \approx \frac{\gamma-1}{4\pi c_0^2}\frac{1}{|\boldsymbol{r}-\boldsymbol{r_0}|}\frac{d\dot{Q}'}{dt} \tag{1}$$

where p' designates the unsteady pressure fluctuations caused by the rate of change of the heat release rate, γ the heat capacity ratio, c_0 the speed of sound between the flame and the measurement point, $\dot{Q}'$ the integrated unsteady heat release rate of the flame, and $\boldsymbol{r}$ and t are the spatial and temporal variables. In principle only valid in the far-field of a compact flame, this expression has been used under similar conditions with some success by several authors [17–20] to estimate the near-field pressure perturbations. Using the data recorded in the ignition sequence of SICCA-spray (Fig. 11), $d\dot{Q}'/dt$ can be roughly estimated at 5 MW s^{-1}, thus the unsteady pressure perturbation at the injector outlet reaches a typical value of approximately 2 kPa.

This rise in pressure downstream of the injection unit corresponds to a decrease in pressure difference across the injector, leading to a drop in air mass flowrate observed in Fig. 11. The flame can then flashback in the injector, meaning that it reaches zones where the velocity is much lower than in the vicinity of the injector outlet. The pressure perturbation lasts $\tau_{\Delta P} = 4$ ms at which point a minimum of inlet flow velocity is reached. This instant corresponds to the maximum of the slope of the time evolution of the heat release rate. The flow velocity within the injector will then relax to its nominal value. The flame will be destabilized and convected at a finite velocity downstream of the injection unit, reaching its final position.

The relaxation of the air flowrate from its perturbed state to its nominal value is a function of injector geometry and flow conditions. This will induce a delay τ_{v_*}, defined as the response time of the injector to return to its nominal value at the end of the pressure perturbation. This delay can be estimated to be less than 1 ms from Fig. 11. Important parameters controlling this relaxation are the pressure loss in the injector and the volume of air that is perturbed by the pressure wave. A framework for the injector dynamics can be derived to represent changes in the air flowrate. It is expressed in a dimensionless form using $v_* = u/u_0$, the reduced velocity at the location of the hot wire probe. One may first consider the conservation of momentum in the injection system and write a first model thereafter called model "M1"

$$\tau\frac{dv_*}{dt} + \frac{1}{2}v_*^2 = \frac{1}{2} + \frac{\Delta p'}{\sigma\rho u_0^2} \tag{2}$$

where $\tau = l/(u_0\sigma)$ is a characteristic time corresponding to the ratio of the length l of the air column displaced by the perturbation by the steady-state velocity measured by the hot wire probe $u_0 = 2.06$ m s^{-1} multiplied by σ a head loss factor defined in Eq. (3). The difference $\Delta p'$ represents a pressure perturbation acting on the system at the injector outlet. This perturbation level and waveshape cannot be determined from the measurements performed in the present study. Using the estimation made from experimental data, it will be modeled as a triangular short pulse with a minimum $\Delta p'_{max} = -2.0$ kPa at $t = 4$ ms followed by a sharp return to zero as shown in black in Fig. 13.

One may take $\rho = 1.2$ kg/m^3 as temperature and mean pressure in the plenum are considered to be near atmospheric conditions. The head loss coefficient $\sigma = 2.39 \times 10^3$ can be evaluated from the usual head loss scaling law (see Fig. 12)

$$\Delta p = \frac{1}{2}\sigma\rho u^2 \tag{3}$$

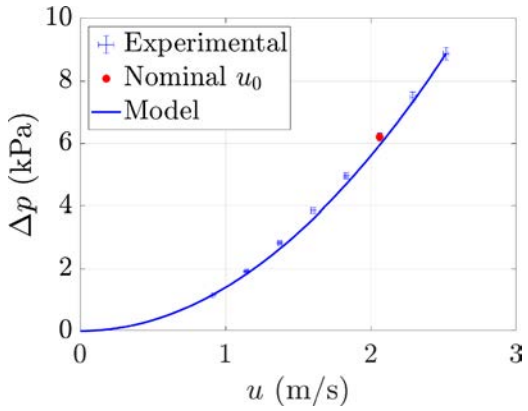

Fig. 12 Pressure loss measurements in the SICCA-spray burner as a function of the velocity at the hot-wire probe position. The values are fitted with the model of Eq. (3). The value at the nominal operating conditions is indicated by a red dot.

Equation (2) can be integrated to determine the air flowrate dynamics. The velocity at the hot wire probe position is initiated at its nominal unperturbed value $u = u_0 = 2.06\,\mathrm{m\,s^{-1}}$ so that $v_*(t=0) = 1$. The results are shown in blue in Fig. 13. The injector flowrate quickly responds to the pressure perturbation, with a 95% response time of 0.35 ms. The initial drop in inlet velocity, which follows the pressure perturbation, is well retrieved: $u_{M1}^{\min} = 1.69\,\mathrm{m\,s^{-1}}$ and $u_{\exp}^{\min} = 1.55\,\mathrm{m\,s^{-1}}$, but the subsequent behavior and oscillations are not.

In the unfiltered curves in Fig. 11, oscillations at $f_0 = 600$ Hz can be observed. This frequency roughly corresponds to the longitudinal quarter wave acoustic mode of the combustion chamber of the SICCA-spray burner, assuming a homogeneous temperature field of 950 K in the combustion chamber, which was preheated before the ignition sequence. To account for the oscillations in flowrate seen in the unfiltered curves in Fig. 11, a second model called model "M2" may be employed that comprises a second-order term

$$\frac{1}{\omega_0^2}\frac{d^2 v_*}{dt^2} + \tau\frac{dv_*}{dt} + \frac{1}{2}v_*^2 = \frac{1}{2} + \frac{\Delta p'}{\sigma\rho u_0^2} \tag{4}$$

In this expression, $\omega_0 = 2\pi f_0$ is the angular frequency. Equation (4) integrated with the initial conditions $dv_*/dt = 0$ and $v_* = 1$ yields the results plotted in Fig. 13. The system behaves quite similarly to model M1 but exhibits an oscillation at 600 Hz. This oscillation, of acoustic origin, is damped, but in model M2 only the contribution of the injector to the acoustic damping is taken into account. Neither model retrieves the low frequency oscillations at 60 Hz of the flowrate observed in Fig. 11. This is probably due to the approximate waveform assigned to the perturbed pressure term. However, these models account for the sudden reduction in flow velocity inside the injector and rapid return to equilibrium. In addition, model M2 accounts for the high frequency oscillations around the steady-state. The delay τ_{v_*} required for the perturbed injector flowrate to reach its steady-state at the end of the pressure perturbation is shown to be small and of the order of 0.4 ms.

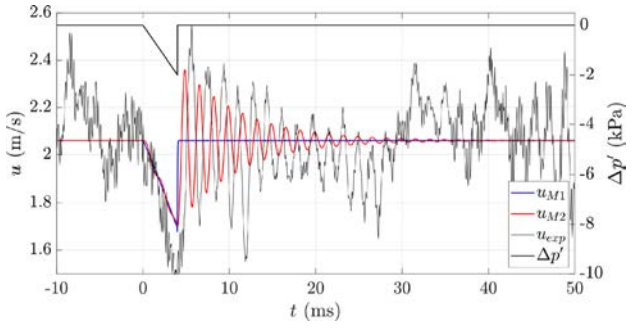

Fig. 13 Velocity obtained at the hot wire position using model M1 (blue, Eq. (2)) and M2 (red, Eq. (4)). The velocity measured by the hot wire is shown as a thin black line. The pressure perturbation used for the present calculation is shown as a thicker black line on top, associated with the right axis. See online figure for color.

6.3 Effects of Local Thermal Conditions. The third factor influencing the flame structure evolution is linked to the thermal conditions characterizing the flame neighborhood. It is well known that flames are sensitive to thermal conditions prevailing near the injector exhaust and at the surrounding boundaries. For example, the light-round time delay is modified if the chamber walls are cold [1]. Experiments [21] and large eddy simulations calculations [22] have shown the influence of the boundary conditions of the chamber walls on the flame shape. Temperature measurements with thermocouples and thermochromic paint have been performed in the annular and tubular experiments under the same injection conditions (results not shown here). They indicate a maximum temperature of 900 K on the outer part of the wall and 1200 K on the inner part of the wall. These temperatures are reached after 10 min of operation. Note that the present experiments are all run under preheated conditions except for experiments in Fig. 4. For all other experiments, the chamber has been run for several minutes to keep the walls at the stabilized thermal conditions. The thermal inertia of the walls is large compared to the transient phenomena observed with the flames.

However, the wall temperature is much lower than the adiabatic flame temperature. The flame shape will be substantially different if the walls are nearly adiabatic or if they are isothermal and at low temperature. One of the mechanisms involved is that the burnt gases are cooled in the outer recirculation zone (ORZ) before reaching the anchoring point of the flame. Under certain conditions depending on a Karlovitz number (linking a turbulent time associated with the recirculation zone and the chemical time), if this Karlovitz number exceeds a critical value [23], the flame front can no longer attach to the lip of the injector. The outer part of the flame then detaches and lifts-off. In the present context, the burnt gases in the ORZ are initially not cooled by the wall, and therefore, can be considered as adiabatic. The flame is then anchored at the lips of the injector. Following this first instant, the burnt gases recirculate in the outer recirculation zone and cool down. These cooled burnt gases will then affect the lower part of the flame, and more specifically, the anchoring point. Several residence times characterize this cooling process and its effect on stabilization.

The residence time of the burnt gases in the ORZ can be evaluated by extrapolating from results in Ref. [21]. In this paper, the swirled flame has a similar aspect to that of this study, and the authors measured the residence time using particle image velocimetry. By normalizing the injector bulk velocity and the confinement ratio, the residence time in the SICCA-spray setup used in the present study can be estimated: $\tau_{\mathrm{ORZ}} = 7$ ms. A multiple of this residence time is required for all thermal processes to reach a steady-state and for the anchoring of the flame to be affected. It should be noted that the thermal equilibrium time delay starts as soon as the combustor is ignited and that this time delay is superimposed to the injector dynamics effects presented in Sec. 6.2.

6.4 Time Delay of the Mechanisms. There is some evidence that each of the three mechanisms mentioned at the beginning of Sec. 6 plays a role in the change in flame structure that is observed. It is, however, difficult with the experimental data from this study to evaluate the contribution of each individual mechanism. Only characteristic time delays have been evaluated with some level of confidence, and the overall time delay $\tau_f = 50$ ms is probably the sum of the individual contribution of each of these mechanisms. The characteristic time delay associated with the fuel droplets is 2 ms. The response of the injector to the pressure

perturbation caused by the ignition spans 5 ms and is probably responsible for the flashback of the flame. The time delay required for the thermal equilibrium to be reached in the ORZ is a multiple of τ_{ORZ}. From this, it can be estimated that five to seven residence times are required for the ORZ to fully thermalize, since $\tau_{ORZ} \approx 7$ ms. This thermal process is most likely responsible for the lift-off of the flame and the overall time delay $\tau_f = 50$ ms required for the flame to reach its final position and shape.

7 Conclusions

This investigation is focused on the dynamics of the flame during the light-round process in annular combustors and specifically considers the evolution of the flame structure established by each injector after it is swept by the traveling flame front. Velocity field measurements indicate that there are two major regions of propagation. In the first, near the combustion backplane, the flow essentially takes place in the azimuthal direction. In this region, the flame sweeps various injectors that are ignited sequentially. In the second region, the reactive front is moving in the azimuthal and axial directions due to the volumetric expansion induced by combustion.

It is next shown that the traveling flame has a strong effect on the flow well before it reaches the point of observation. This is due to the piston effect associated with the volumetric expansion induced by the flame. The flow in front of the flame is set into motion and the spray of droplets delivered by a given injector is blown sideways. One may infer from this observation that the local equivalence ratio is perturbed, with a possible creation of heterogeneous regions. These different features do not depend on the observation point and are valid for a large number of injectors, except those near the initiation of the combustion process, at the spark plug and those located near the merging point of the two traveling flame branches where the flow is severely perturbed.

A third observation indicates that the azimuthal sweeping of an injector by the combustion wave establishes a flame that is initially penetrating the injector unit. This flame is then expelled from this region and after a certain delay is anchored at its final position. This dynamical behavior is of practical importance because it indicates that prior to the stabilization at a distance from the injection unit, the flame takes positions that may damage the injector. Of course, this is only a model scale version of what is being used in real systems but it shows that some attention needs to be given to the injector dynamics as it is swept by the combustion wave traveling in the chamber. Similar features are observed when a single injector is ignited by a spark plug.

Several mechanisms are involved in this transient phenomenon, including equivalence ratio disturbances, sudden reduction in the air flowrate caused by the unsteady pressure excursion during ignition, and thermal delays in the outer recirculation zone. The dynamics of the injector response is examined by considering a simplified model representing the mass flowrate evolution after the initial disturbance induced by the sweeping of the combustion wave which induces a large negative disturbance in the mass flowrate. The velocity in the unit is reduced and allows the penetration of the flame front. The injector then rapidly responds to this perturbation by retrieving the steady-state mass flowrate and the flame is expelled from this unit. Calculations based on a simplified model retrieve the aerodynamic behavior of the injector following the ignition. After a further delay required to fully thermalize gases in the outer recirculation zone, the flame reaches its final shape. Time delays associated with each mechanism are estimated and the overall time delay is retrieved.

Acknowledgment

This work was supported by Safran Tech, CNRS and ANR (Timber project ANR14-CE23-0009-01). The authors wish to thank J. Beaunier and Y. Le Teno for the technical support provided to this research. They also wish to thank Drs. Ronan Vicquelin and Thea Lancien for helpful discussions. Finally, they want to thank Ametek and Vision Search for the use of the high-speed camera Phantom V2512.

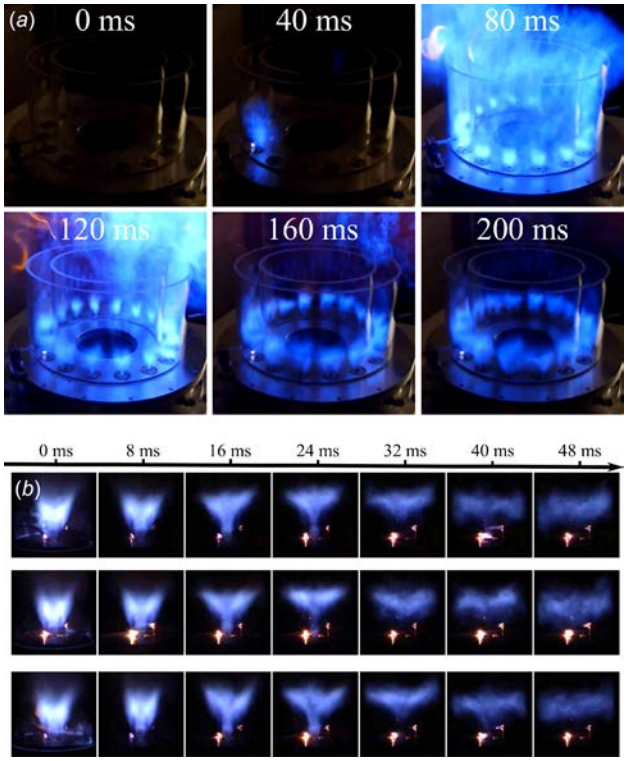

Fig. 14 Top: True-color low-speed images of the light-round in the MICCA combustion chamber under premixed propane-air conditions with $\phi = 0.76$ and $\mathcal{P} = 60$ kW. Bottom: Three ignition sequences of the SICCA burner equipped with the premixed swirled injector with $\phi = 0.76$ and $\mathcal{P} = 3.75$ kW.

Appendix: Flame Shape in Multiple Injector Combustor for Combustion Dynamics and Acoustic Analysis

It is interesting to see whether the evolution of flame shapes observed in a swirl spray configurations can also be observed in the case of fully premixed gaseous injection. The spray injectors are replaced by premixed injectors with a slightly different swirler geometry as in Ref. [5] but having about the same swirl number $S \approx 0.7$. Figure 14 shows at the top the ignition of the annular combustor with these injectors for a propane/air mixture at $\phi = 0.76$ and $\mathcal{P} = 60$ kW. One can see that flames at 120 ms and 160 ms are quite different. The same injection system is mounted on the SICCA single injector tubular burner to examine the ignition steps. As for the spray injector, the flame is first quite compact and moves into the injection system before stabilizing and being lifted at about 40 ms. This indicates that the phenomenon observed in this study is not specific to spray swirl injection configurations.

References

[1] Prieur, K., Durox, D., Beaunier, J., Schuller, T., and Candel, S., 2017, "Ignition Dynamics in an Annular Combustor for Liquid Spray and Premixed Gaseous Injection," Proc. Combust. Inst., **36**(3), pp. 3717–3724.

[2] Cordier, M., Vandel, A., Renou, B., Cabot, G., Boukhalfa, M. A., Esclapez, L., Barre, D., Riber, E., Cuenot, B., and Gicquel, L., 2013, "Experimental and Numerical Analysis of an Ignition Sequence in a Multiple-Injectors Burner," ASME Paper No. GT2013-94681.

[3] Barre, D., Esclapez, L., Cordier, M., Riber, E., Cuenot, B., Staffelbach, G., Renou, B., Vandel, A., Gicquel, L. Y. M., and Cabot, G., 2014, "Flame Propagation in Aeronautical Swirled Multi-Burners: Experimental and Numerical Investigation," Combust. Flame, **161**, pp. 2387–2405.

[4] Bach, E., Kariuki, J., Dawson, J. R., Mastorakos, E., and Bauer, H.-J., 2013, "Spark Ignition of Single Bluff-Body Premixed Spark Ignition of Single Bluff-Body Premixed," AIAA Paper No. 2013-1182.

[5] Bourgouin, J. F., Durox, D., Schuller, T., Beaunier, J., and Candel, S., 2013, "Ignition Dynamics of an Annular Combustor Equipped With Multiple Swirling Injectors," Combust. Flame, **160**(8), pp. 1398–1413.

[6] Machover, E., and Mastorakos, E., 2015, "Spark Ignition of Annular Non-Premixed Combustors," Exp. Therm. Fluid Sci., **73**, pp. 64–70.

[7] Boileau, M., Staffelbach, G., Cuenot, B., Poinsot, T., and Berat, C., 2008, "LES of an Ignition Sequence in a Gas Turbine Engine," Combust. Flame, **154**(1–2), pp. 2–22.

[8] Philip, M., Boileau, M., Vicquelin, R., Schmitt, T., Durox, D., Bourgouin, J. F., and Candel, S., 2014, "Ignition Sequence in a Multi-Injector Combustor," Phys. Fluids, **26**(9), p. 091106.

[9] Philip, M., Boileau, M., Vicquelin, R., Riber, E., Schmitt, T., Cuenot, B., Durox, D., and Candel, S., 2015, "Large Eddy Simulation of the Ignition Sequence of an Annular Multiple Injector Combustor," Proc. Combust. Inst., **35**(3), pp. 3159–3166.

[10] Philip, M., Boileau, M., Vicquelin, R., Schmitt, T., Durox, D., Bourgouin, J. F., and Candel, S., 2014, "Simulation of the Ignition Process in an Annular Multiple-Injector Combustor and Comparison With Experiments," ASME J. Eng. Gas Turbines Power, **137**(3), p. 031501.

[11] Lancien, T., Prieur, K., Durox, D., Candel, S., and Vicquelin, R., 2017, "Large Eddy Simulation of Light-Round in an Annular Combustor With Liquid Spray Injection and Comparison With Experiments," ASME J. Eng. Gas Turbines Power, **140**(2), p. 021504.

[12] Machover, E., and Mastorakos, E., 2017, "Numerical Investigation of the Stochastic Behavior of Light-Round in Annular Non-Premixed Combustors," Combust. Sci. Technol., **189**(9), pp. 1467–1485.

[13] Thielicke, W., and Stamhuis, E., 2014, "PIVlab–Towards User-Friendly, Affordable and Accurate Digital Particle Image Velocimetry in MATLAB," J. Open Res. Software, **2**(1), p. e30.

[14] Mirat, C., Durox, D., and Schuller, T., 2014, "Analysis of the Spray and Transfer Function of Swirling Spray Flames From a Multi-Jet Steam Assisted Liquid Fuel Injector," ASME Paper No. GT2014-25111.

[15] Mirat, C., Durox, D., and Schuller, T., 2015, "Stability Analysis of a Swirl Spray Combustor Based on Flame Describing Function," Proc. Combust. Inst., **35**(3), pp. 3291–3298.

[16] Prieur, K., Durox, D., Schuller, T., and Candel, S., 2017, "Strong Azimuthal Combustion Instabilities in a Spray Annular Chamber With Intermittent Partial Blow-Off," ASME J. Eng. Gas Turbines Power, **140**(3), p. 031503.

[17] Strahle, W. C., 1978, "Combustion Noise," Prog. Energy Combust. Sci., **4**(3), pp. 157–176.

[18] Schuller, T., Durox, D., and Candel, S., 2003, "Self-Induced Combustion Oscillations of Laminar Premixed Flames Stabilized on Annular Burners," Combust. Flame, **135**(4), pp. 525–537.

[19] Candel, S., Durox, D., and Schuller, T., 2004, "Flame Interactions as a Source of Noise and Combustion Instabilities," AIAA Paper No. 2004-2928.

[20] Noiray, N., Durox, D., Schuller, T., and Candel, S., 2007, "Passive Control of Combustion Instabilities Involving Premixed Flames Anchored on Perforated Plates," Proc. Combust. Inst., **31**(1), pp. 1283–1290.

[21] Guiberti, T., Durox, D., Scouflaire, P., and Schuller, T., 2015, "Impact of Heat Loss and Hydrogen Enrichment on the Shape of Confined Swirling Flames," Proc. Combust. Inst., **35**(2), pp. 1385–1392.

[22] Maio, G., Cailler, M., Mercier, R., and Fiorina, B., 2018, "Virtual Chemistry for Temperature and CO Prediction in LES of Non-Adiabatic Turbulent Flames," Proc. Combust. Inst. (in press).

[23] Guiberti, T., Durox, D., Zimmer, L., and Schuller, T., 2015, "Analysis of Topology Transitions of Swirl Flames Interacting With the Combustor Side Wall," Combust. Flame, **162**(11), pp. 4342–4357.